

NULL TRANSITION TIMES, QUANTIZED DRIFT MODES, AND NO MEMORY ACROSS
NULLS FOR PSR 1944+17

W. T. S. DEICH

Astronomy Department, Cornell University

J. M. CORDES

Astronomy Department, Cornell University and National Astronomy and Ionosphere Center

T. H. HANKINS

School of Engineering, Dartmouth College

AND

J. M. RANKIN

Physics Department, University of Vermont

Received 1984 April 10; accepted 1985 July 18

ABSTRACT

Intensity nulling and subpulse drifting have been examined in detail for a pulsar that shows no detectable emission (nulls) in $\sim 60\%$ of pulse periods. Three drift modes occur, two of which display a 1:2 ratio of drift rates, while the third mode has zero drift rate. A fourth mode, characterized by chaotic subpulse phase, is also observed. Nulls disrupt the more organized drift modes, but null transitions are often preceded by a change from organized to chaotic drift. We find no evidence for memory of subpulse phases across nulls, a result that contrasts with the memory observed for PSR 0809+74 by Unwin *et al.* We find significant differences in amplitude and shape between the last pulse *before* a null and other pulses with detectable emission. However, the first pulse *after* a null has a wave form only slightly different than the average wave form. A null appears as a modulation of pulsar emission with two characteristic time scales: a decrease of flux density by $\sim 50\%$ over several pulse periods, followed by a rapid transition to zero measurable emission on a time scale less than or equal to one subpulse decay time. The transition from null to burst is also characterized by a 2–30 ms transition time. We discuss these results with reference to recent models involving modulations of pair production cascades and magnetospheric structure.

Subject heading: pulsars

I. INTRODUCTION

Subpulse drift, in which features in individual pulses systematically change phase from pulse period to pulse period, was recognized in early studies of single pulses (Drake and Craft 1968). Fluctuation spectra and correlation function analyses show that drifting is highly organized in some objects, occurs intermittently in others, and for others occurs with quantized values of the drift rate (Huguenin, Taylor, and Troland 1970; Taylor and Huguenin 1971; Backer 1970). Unwin *et al.* (1978) showed for PSR 0809+74 that drift ceases, to first order, during a null. (A null is the absence of detectable radio emission for one or more pulse periods.) This discovery showed that nulling is intimately connected with drifting, and therefore the cause of drift can, in some instances, be related to the establishment of coherent radio emission.

More recent work on PSR 0809+74 (Popov and Smirnova 1982; Filippenko, Readhead, and Ewing 1983; Lyne and Ashworth 1983) has shown that the average drift occurring across a null (i.e., the change in pulse longitude from the last pulse before the null to the first pulse after the null) is approximately the same as the average drift that occurs in one pulse period during a burst, where a burst is a string of consecutive pulses above some detection threshold. The average drift rate during nulls decreases with null length. Following a null, the drift rate is initially less than average and then exponentially relaxes to the normal rate. This result constrains possible models for emission mechanisms, since any successful model must predict

both the continuous drift that often occurs during a burst and the relatively small amount of drift across a null.

We have studied the behavior of the drifting subpulses and nulling in PSR 1944+17 ($P = 0.441$ s), an object which allows a large number of null transitions to be examined, since 60% of the pulses are null pulses. Burst pulses are often very intense, and the drift behavior is rich in phenomena, so PSR 1944+17 is well suited for a study of the interaction of drifting and nulling. We find no evidence for phase memory, but there are differences between the last pulse before a null and the other pulses in a burst. We also find two time scales for the onset of a null. There is a decline of the pulse intensity for several pulse periods, followed by a rapid drop to the null state on a time scale $2 \text{ ms} < \tau < 30 \text{ ms}$. We briefly discuss the implications of our measurements in terms of polar cap models.

II. METHOD OF ANALYSIS

Several groups of observations were made at Arecibo between 1972 and 1981 at 430 and 1420 MHz, using sample intervals ranging from 300 to 800 μs . Figure 1 shows a typical pulse sequence at 430 MHz in which nulls and intense pulses are evident.

Figure 2 shows a bar graph of the lengths of successive bursts and nulls. The average burst length is 13 pulse periods, and the average null length is 19 pulse periods. Actual burst and null lengths range from one to several hundred periods. As Figure 2 illustrates, there are several places where bursts

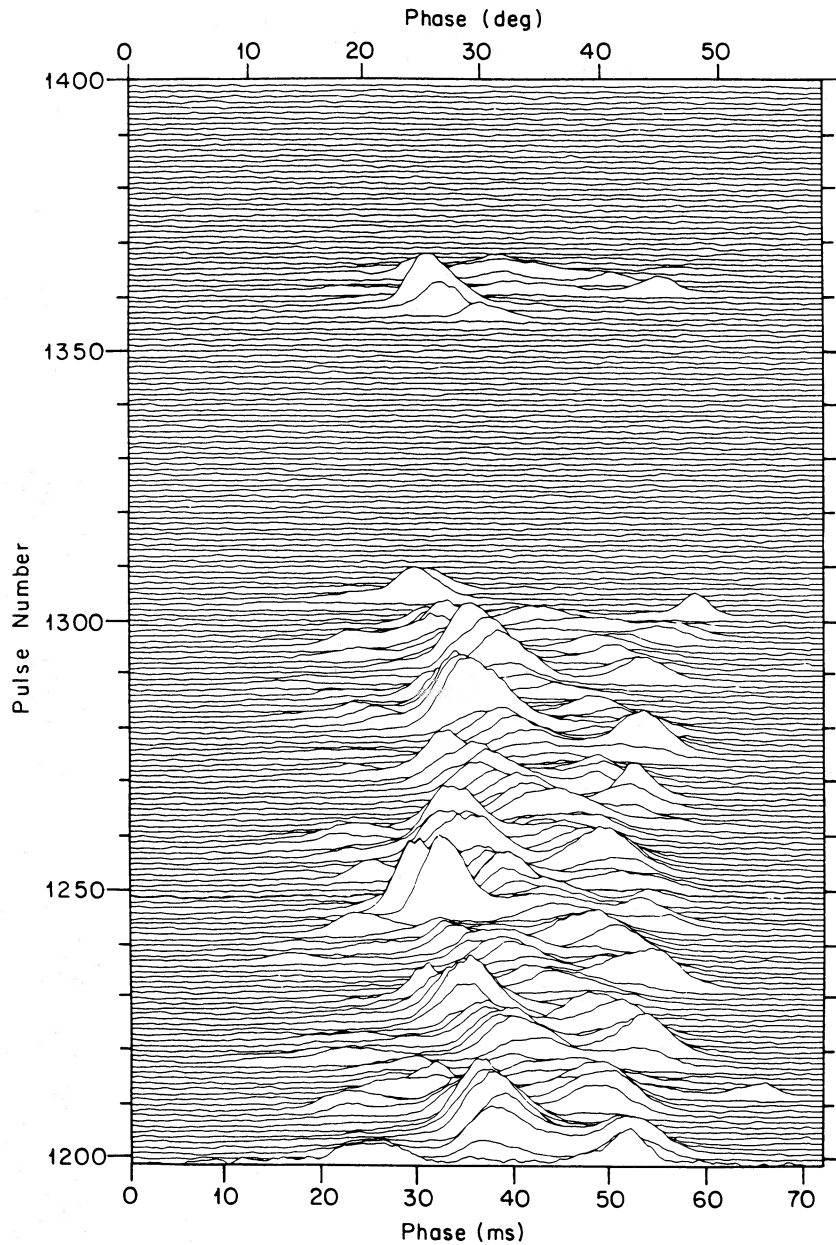


FIG. 1.—Plot of pulse number vs. longitude for approximately 200 pulses. Both nulls and intense pulses are evident.

appear to be interrupted by single nulls, involving intensity changes of as much as a factor of 200.

We defined an “ON” window to be centered on the average pulse profile, spanning a region approximately twice its FWHM. The “OFF” window was defined to be a block of samples well-separated from the ON region. Off-pulse noise levels were determined by averaging over the OFF regions of null pulses only. Typical burst pulses have peak flux densities of ~ 200 times the rms noise level after smoothing over one subpulse width. Approximately 64% of all pulses are nulls, using a 5σ detection threshold.

Burst pulses were identified by convolving the ON region with a unit area boxcar whose duration was approximately equal to the subpulse width ($\text{FWHM} \approx 21$ ms). This estimate for the width is based on the average autocorrelation function (ACF) of burst pulses. We used $\text{FWHM}(\text{subpulse}) \approx$

$(1/2^{1/2})\text{FWHM}(\langle \text{ACF} \rangle)$. If any point in the convolution was above the 5σ detection threshold, we concluded that the pulsar was “on.” The distribution of the average flux density in burst pulses is shown in Figure 3 for both ON- and OFF-pulse regions. The overlap between the two prevents one from unambiguously distinguishing bursts from nulls but an average wave form of null pulses (also shown in Fig. 3) is very nearly consistent with noise, indicating that any misidentifications are rare.

III. DRIFTING SUBPULSE MODES

a) Drift Patterns within Bursts

It is obvious from Figure 4 that the drift rate and coherence of the drift are highly variable from one burst to another. Following conventional notation (e.g., Manchester and Taylor 1977) we characterize drift bands with the quantities P_2 , the

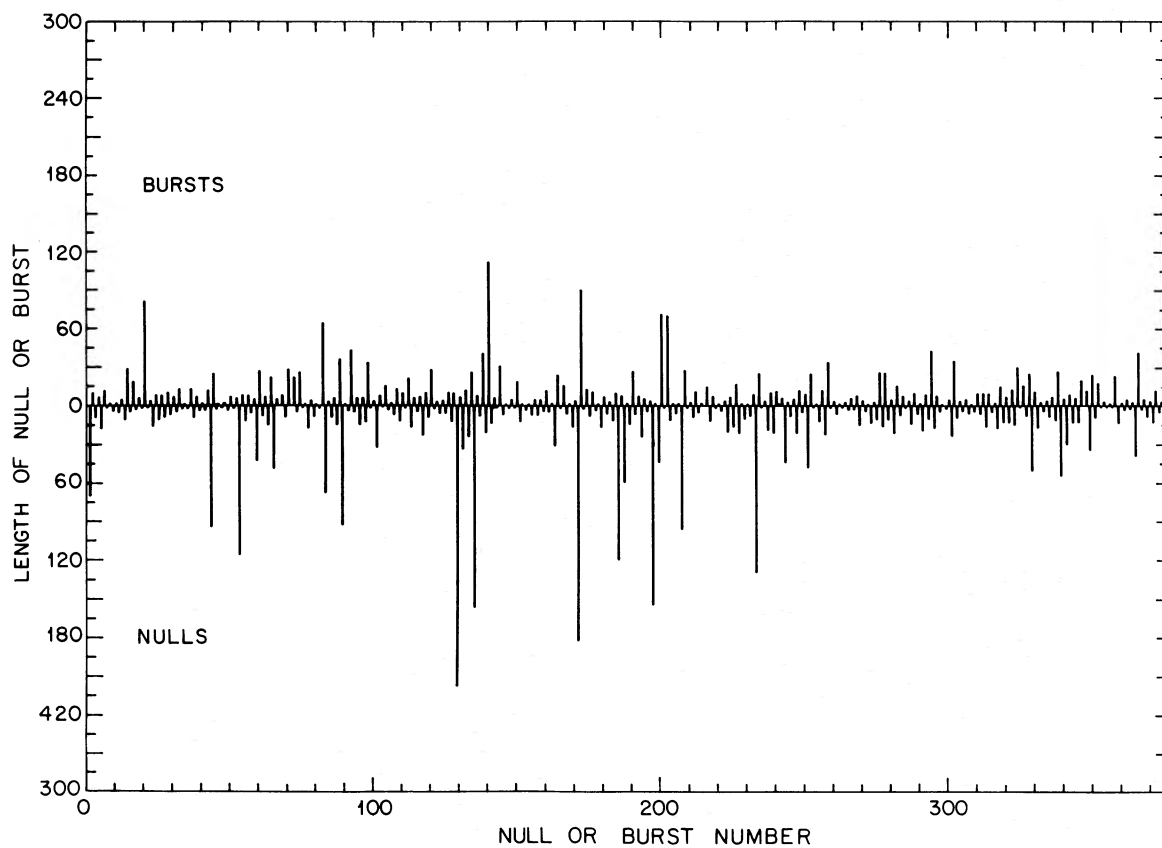


FIG. 2.—Lengths of bursts and nulls: a group of some 380 successive bursts and nulls are shown. Lengths of bursts are represented by length of the bar extending up from the horizontal axis; null lengths are shown as bars extending below the axis.

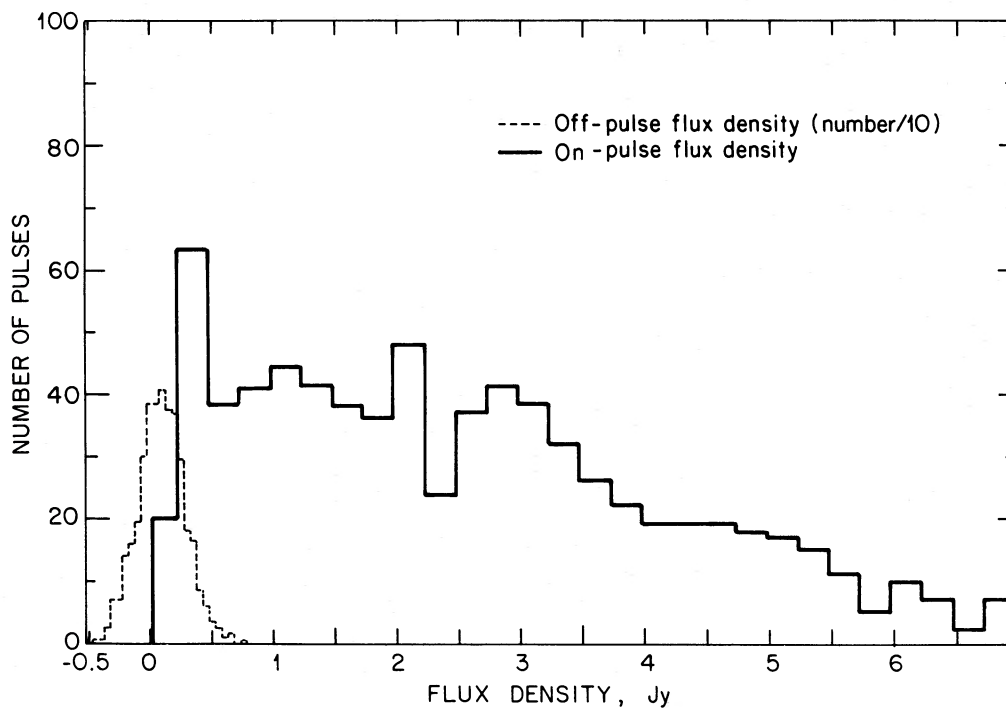


FIG. 3.—Distribution of average flux density in burst pulses for both the ON and OFF pulse regions. Counts for the OFF region have been divided by 10.

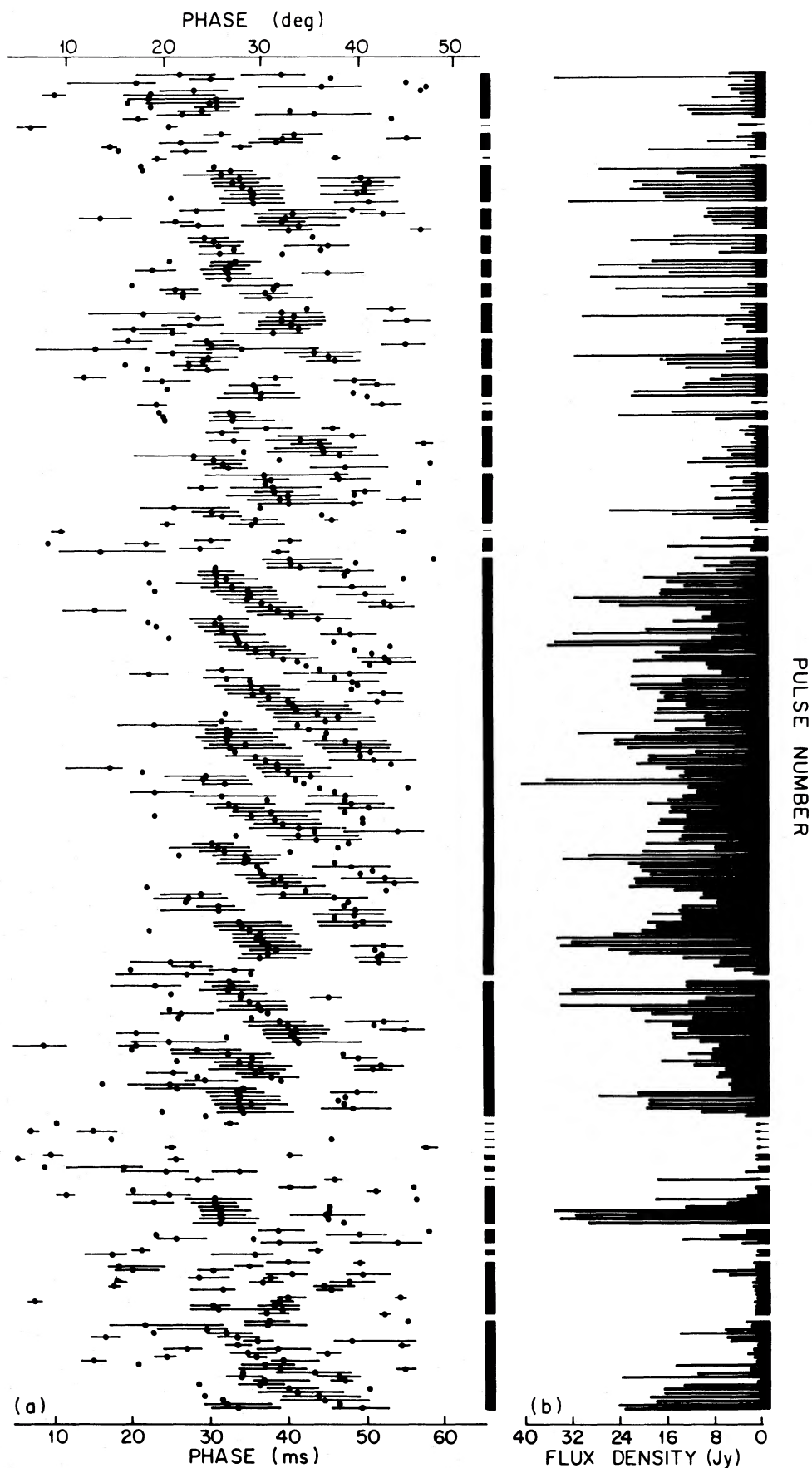


FIG. 4.—A sequence of ~ 1400 pulses. (a) Only subpulse peaks are shown here. Nulls have been removed from the plot; their positions are indicated by the blanks between bursts. Heavy superimposed bars are the FWHM of the subpulse, if one could be found. (b) Average flux density in the largest subpulse of each pulse.

TABLE 1
DRIFT MODES IN PSR 1944+17

Parameters	430 MHz	1420 MHz
Mode A:		
P_2 (ms)	13.6 ± 1.7	12.2 ± 1.6
P_3 (periods)	14.1 ± 2.6	13.0 ± 2.3
Drift rate ($= P_2/P_3$)	0.96	0.94
(ms/period)		
Number of bursts	15	26
Number of drift bands	42	91
Mode B:		
P_2 (ms)	12.5 ± 1.8	11.2 ± 1.3
P_3 (periods)	6.3 ± 1.0	6.4 ± 1.4
Drift rate ($= P_2/P_3$)	1.98	1.75
(ms/period)		
Number of bursts	9	15
Number of drift bands	22	31
Relative frequency of occurrence:		
mode A/mode B	1.9	2.9

separation of subpulses within a given pulse period, and P_3 , the separation between drift bands at fixed pulse phase. We analyzed 10^4 periods of data from both 430 and 1420 MHz in three ways in order to obtain statistics on P_2 , P_3 , and drift rate.

1. The quantities P_2 and P_3 were first measured by fitting straight lines by eye to the pulse peaks of gray scale plots of intensity versus pulse number and pulse phase. Only those bursts in which there were at least three clear drift bands were used. The quantity P_2 was then scaled from the plots as the separation in pulse phase between the straight lines, and P_3 was obtained by measuring the number of periods between intersections of the fit lines and the peak phase of the average profile. The values obtained are presented in Table 1. We also list the number of bursts and number of drift bands whose drift parameters could be measured by this method.

2. Method 1 above is strongly biased toward drift patterns that are regular and periodic and therefore easily recognized by eye. It produces stable and definite values for P_2 and P_3 .

Our second analysis was designed to measure the relative frequency of drift bands of arbitrary drift rate. The gray scale plots were examined for subpulses whose longitude appears to the eye to be correlated over four or more periods, without regard to magnitude or sign of the drift, and without comparing the apparent drift rate with other "nearby" drift bands. We show a histogram of the drift rates of these drift bands in Figure 5.

Three different kinds of drift patterns were found. The first, which we call mode A (following the convention of Wright and Fowler 1981) is characterized by $P_3 \approx 14$ periods and a drift rate of $(P_2/P_3) \approx 1$ ms per period. Mode A is evident in the long burst in the middle part of Figure 4 and usually appears in the longest bursts that contain 10–15 drift bands. The B mode, with a higher drift rate $(P_2/P_3)_B \approx 2$ ms per period $\approx 2 \times (P_2/P_3)_A$ occurs less than half as often as mode A in bursts that are typically shorter. Many short bursts of 10 periods or less show essentially zero drift, even though subpulses are distinct and are separated by the nominal value of P_2 . We call this mode C. Table 1 gives values for P_2 and P_3 for modes A and B at both radio frequencies. (The data for 430 and 1420 MHz were not obtained simultaneously, so the fact that the relative frequencies of occurrence of the two modes differs at 430 and 1420 MHz can be attributed to small number statistics.)

3. We also subjected the data to an unbiased (but more prone to confusion) computer analysis of subpulse drift which we discuss later.

We note that the apparent widths of the mode A, B, and C features of Figure 5 are considerably wider than one would expect from the estimation errors implied in Table 1. This results from the requirement of method 1 that P_2 and P_3 be measured only for well-organized drift patterns, whereas the selection rules for measuring drift rate in method 2 are much less stringent, since all drift bands, whether they are periodic or not, are included for method 2. This implies that the distribution of P_2/P_3 is narrow for the organized periodic drifts, but that for single drift bands, a much wider range of rates is observed.

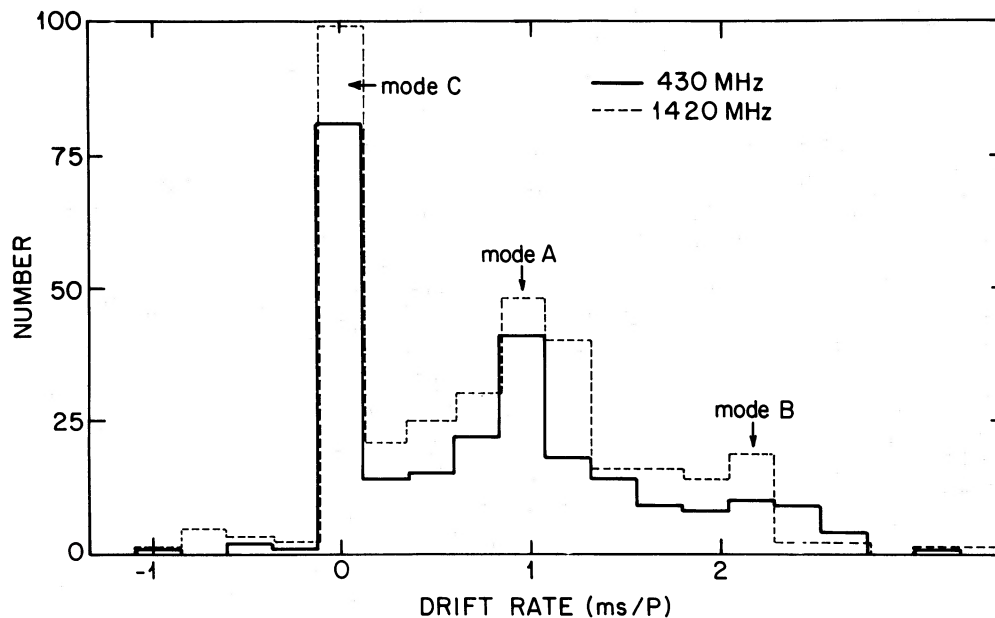


FIG. 5.—Drift rates determined from only those data showing (to the eye) organized drift over four or more pulse periods, as discussed in § III. Arrows designate drift rates for modes A and B.

b) No Memory across Nulls

Transitions between drift modes are correlated with transitions to and from the null state. Modes A and B are almost always separated by a null of many periods, though one case was observed where a change from mode A to B occurred within a single burst. In long bursts, mode A is usually preceded by an episode of mode C that lasts 10 or more periods. No obvious systematic continuity can be seen across nulls with the eye, a result that is confirmed by the numerical analysis discussed below. The eye does pick up apparent alignments across some nulls (e.g., top of Fig. 4), but these seem to be spurious.

The presence of both organized and chaotic drift behavior makes it difficult to establish whether any phase memory is present across nulls. Unwin *et al.* (1978) established such a memory for PSR 0809+74, an object with a much less variable drift rate than that of PSR 1944+17. Visually, we find no evidence for memory across nulls for 1944+17. In order to check our visual impressions, we subjected the data to a cross-correlation analysis, referred to as method 3 above. To follow the drift, we cross-correlated each burst pulse with its neighbor and fitted the cross-correlation function (CCF) with a parabola whose maximum we used to determine the drift rate. Depending on the relative amplitudes of the pair of subpulses that is usually found in a given period, such a procedure can misidentify the subpulse of one period with its neighbor of the next period by finding the local CCF maximum at lag $(P_2 + P_2/P_3)$ rather than the maximum at lag P_2/P_3 . We avoided this problem by using only those local maxima within ~ 6 ms (5° of pulse longitude or phase) of zero lag, since $P_2 \approx 12$ ms, while the drift rate across one pulse period is < 3 ms.

The drift rate for an entire burst was measured by summing the CCF's of all nearest neighbors in that burst and finding the lag of peak correlation. The drift across nulls was measured by cross-correlating the last pulse of one burst with the first pulse of the next. Since 1944+17 has some very long nulls (up to several hundred pulse periods), the drift across nulls is particularly susceptible to misidentification of the proper subpulse (aliasing). To avoid imposing *a priori* assumptions about drift across nulls, we therefore placed no restrictions on which lags were searched for maxima.

Histograms of drift rate are shown in Figure 6. One histogram (Fig. 6a) is the burst-averaged drift rate which shows a peak near the dominant mode A rate. The peak value is slightly lower than the node A value, presumably because the smearing effects of mode C behavior shift the maximum of the average CCF toward zero. The other histogram (Fig. 6b) is the inferred drift rate across nulls. The average drift rate is close to zero, but the spread in values is larger than that for bursts (partly because fewer subpulses contributed to the CCF's, partly because a lack of memory [see below] causes spreading). Since the drift rate across long nulls is forced to be small, this result of zero drift rate may be misleading.

An analysis of the net *drift* (rather than rate) is summarized in Figure 7, which shows (Fig. 7a) separate histograms of subpulse phase for the first and last pulses of a burst. The phase is measured by the centroid of a parabola fitted to the peak of the smoothed pulse profile. If the phases of turn-off and subsequent turn-on are independent random variables, then the probability density function (pdf.) of the net drift between turn-off and turn-on is the phase-reversed cross-correlation function of the pdf.(turn-off) and pdf.(turn-on). This predicted pdf.(after binning) is shown in Figure 7b, along with the actual histogram. There is no significant difference between the two, con-

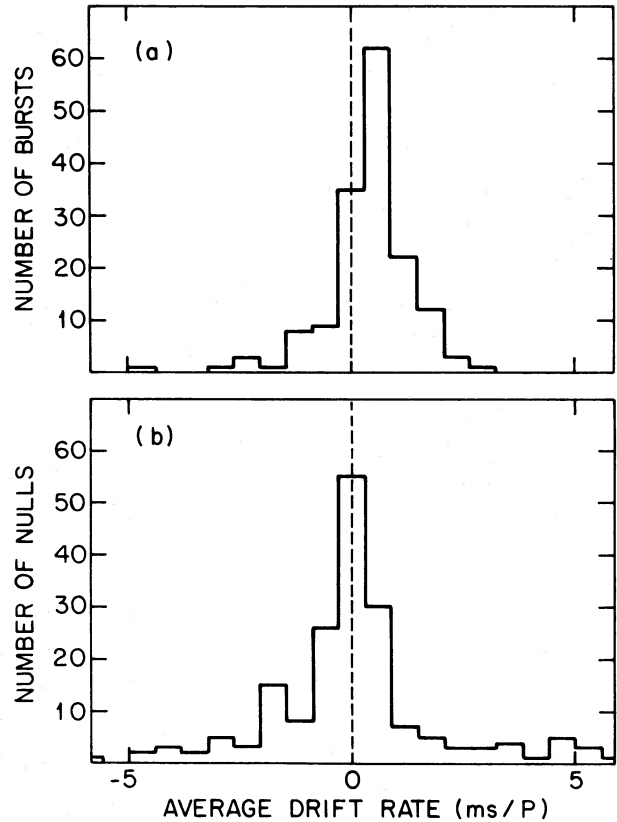


FIG. 6.—Histogram of drifting determined from a cross-correlation analysis on all data. (a) Burst-averaged drift rate. (b) Drift rate across nulls.

firming the visual results that the data are consistent with no phase memory across nulls. A plot of the phase of the last burst pulse against the phase of the first pulse of the next burst (not shown) shows complete scatter. Consideration of only short nulls (less than 10 periods) still shows no correlation: memory does not improve with decreasing null length.

IV. TRANSITION TO THE NULL STATE

In this situation we examine pulse shapes and amplitudes to determine their temporal evolution during a burst and to determine what behavior signifies the onset of a null.

a) Pulse Shapes and Intensities

Average profiles of (1) the initial pulses of bursts, (2) all middle pulses of bursts, and (3) the last pulses of bursts are shown in Figure 8a. (Bursts of only one pulse were lumped under “first” pulses.) Since the middle pulses contain ~ 10 times as many pulses as the other profiles, we divided them into 10 smaller groups to facilitate comparison. The shaded region in Figure 8a indicates the maximum excursion of the 10 subgroups of middle pulses from the average, giving an indication of the intrinsic variations in the average profile of the smaller groups. Approximately 1000 pulses are included in the “middle” average. It is clear that “last” pulses differ substantially in character from “first” and “middle” pulses. The average wave form of pulses that we identified as nulls (Fig. 8a) shows no evidence for significant emission. (The slight increase in the average value in the on-pulse region may be attributed to the occasional very low intensity pulse at the end of a burst being interpreted as the first null pulse rather than the last

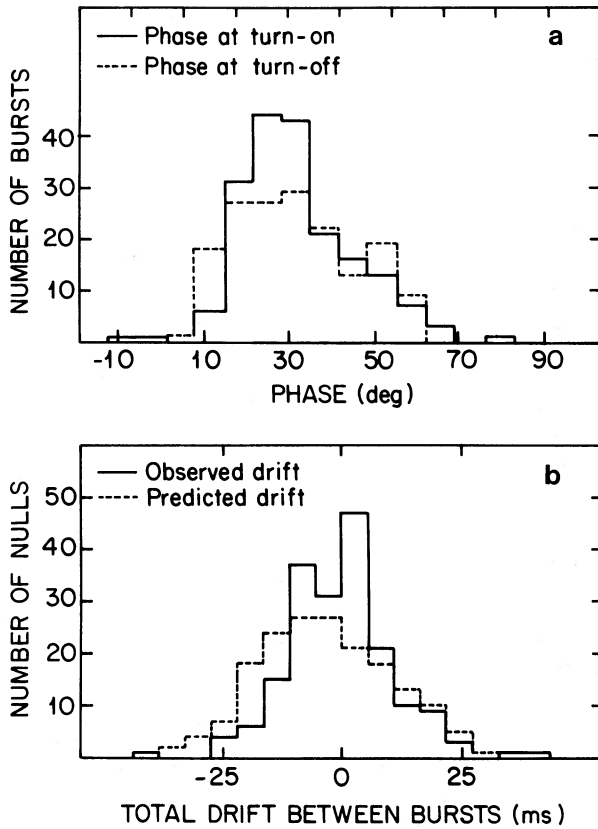


FIG. 7.—(a) Phase histograms of the first pulses in bursts (solid line); the last pulses in bursts (dashed line). Phase origin is arbitrary. (b) Total drift between bursts (solid line); the histogram predicted if there is no “memory” (dashed line).

burst pulse.) The wave form of middle pulses fluctuates in accord with the $1/N^{1/2}$ uncertainty expected when averaging N pulses. The wave form of last pulses, however, shows much larger fluctuations (over and above $1/N^{1/2}$ fluctuations), especially in the ratio of trailing component to leading component, which varies by 25% between averages of 100 last pulses. The autocorrelation functions in Figure 8b for first, middle, and last pulses show the same relative stability as the wave forms. Often, but not always, a subaverage ACF of last pulses is significantly narrower than the ACF’s for the other pulses. We summarize these results by simply saying that last pulses have shapes that are much more variable than those of the other pulses.

b) Null Transition Times

There appear to be two time scales describing the onset of a null: a gradual decrease in flux density over several pulse periods, followed by an abrupt decrease to the null state. Figure 9 shows the signature of pulse energies in bursts and nulls. We averaged over those bursts with more than eight pulses which were followed by at least three null pulses. Shorter bursts were not included, because we wanted to separate long time scale effects occurring at turn-on from those occurring at turn-off.

The average flux density in the final subpulses is ~ 0.5 times that of the middle pulses of a burst, and from Figure 9 we conclude that there is a relatively long decay ($\tau \approx 3P$) in pulse flux density before a null. This long decay time is also evident

in other observations of PSR 1944+17 (e.g., see Fig. 8 of Ritchings 1976).

We now turn to the fast decay. The transition time from final pulse to null cannot be much longer than the subpulse decay time, because the first null pulse has an average flux density that is at least a factor of 50 smaller than the last burst pulse. If the transition time were much longer, the first null pulse would be of higher flux density.

On the other hand, if the turn-on/off time scale was brief compared with the width of a subpulse, and if a subpulse emission region was sweeping past the observer at the turn-on/off time, we would expect to see an unusually sharp edge on the subpulse. Letting Δt be the total width of a subpulse and P be the pulsar period, the probability of observing a sharp edge in a single transition is

$$p_{\text{transition}} \approx \Delta t/P. \quad (1)$$

We observed 400 transitions that could easily be inspected by eye: taking $\Delta t/P \approx 0.05$ and using the Gaussian approximation to the binomial pdf of the number of transitions, we would expect to see $\sim 20 \pm 8$ sharp edges at the 95% confidence interval. We observed no sharp edges. (The relevant “total width” here is defined by the points at which we could see a sharp edge by eye. For the estimate above, we conservatively took the total width to be the subpulse FWHM.) We could have detected decays that occurred in a time less than 2 ms, thus putting a lower limit on the time scale to decay. We quantitatively analyze the situation below.

c) Model for Null Transition

We attempt to model the pulse shape and mean intensity of the last pulse as follows. Let $N(t)$ be the null signature—that is, a function that modulates the emission from the pulsar in the corotating frame and which we consider to be a monotonically decreasing function.

We first consider only the *integrated* pulse energy, so that the wave form shape does not enter the analysis. Suppose the null can begin at any phase, and we sample the emission at discrete times as a consequence of the beaming (ignoring finite pulse widths, drifts, variations in the “ON” flux density, and so on). For a given null, we sample $N(t)$ according to

$$I(k) = I_0 N(kP + t_0), \quad (2)$$

where $I(k)$ is the integrated intensity (over the k th pulse), I_0 = mean burst pulse intensity, and t_0 = null phase. In order to permit us to ignore the slow (several pulse period) decay of the intensity, we consider only the ratio of $I_B(L)$ to $I_N(1)$, where $I_B(L)$ is the intensity of the last burst pulse and $I_N(1)$ is the intensity of the first null pulse. Since the slow decay time is larger than one pulse period, it does not substantially affect the pulse shape over one period and hence does not affect the *ratio* of intensities.

According to our detection criteria, a pulse with $I(k) < I_T$ (I_T = the threshold intensity for detection) is considered a null pulse, so the ratio $I_B(L)/I_N(1)$ depends on the phase t_0 , as well as on the signature $N(t)$. We want the average value of this ratio; $I_0 N(t)$ can fall below threshold at any phase, so the mean intensity of the first null pulse is

$$\langle I_N(1) \rangle = \frac{1}{P} \int_{t_T}^{t_T+P} I_0 N(t) dt, \quad (3)$$

where t_T is defined by $I_0 N(t_T) = I_T$. Similarly, the mean inten-

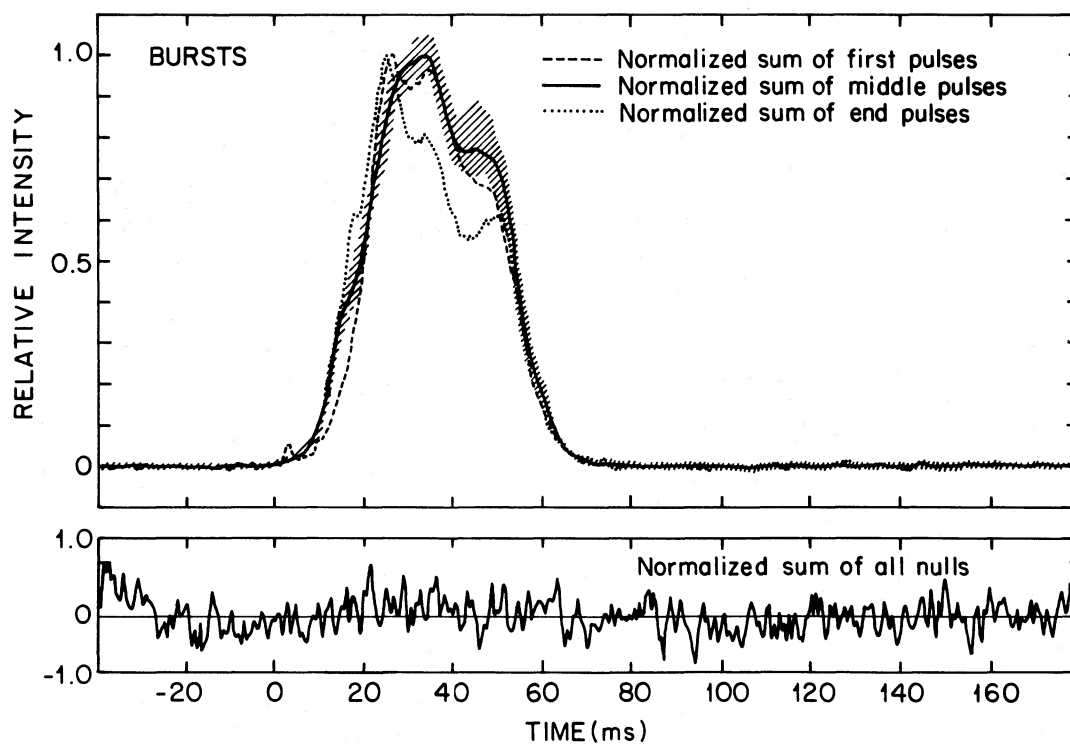


FIG. 8a

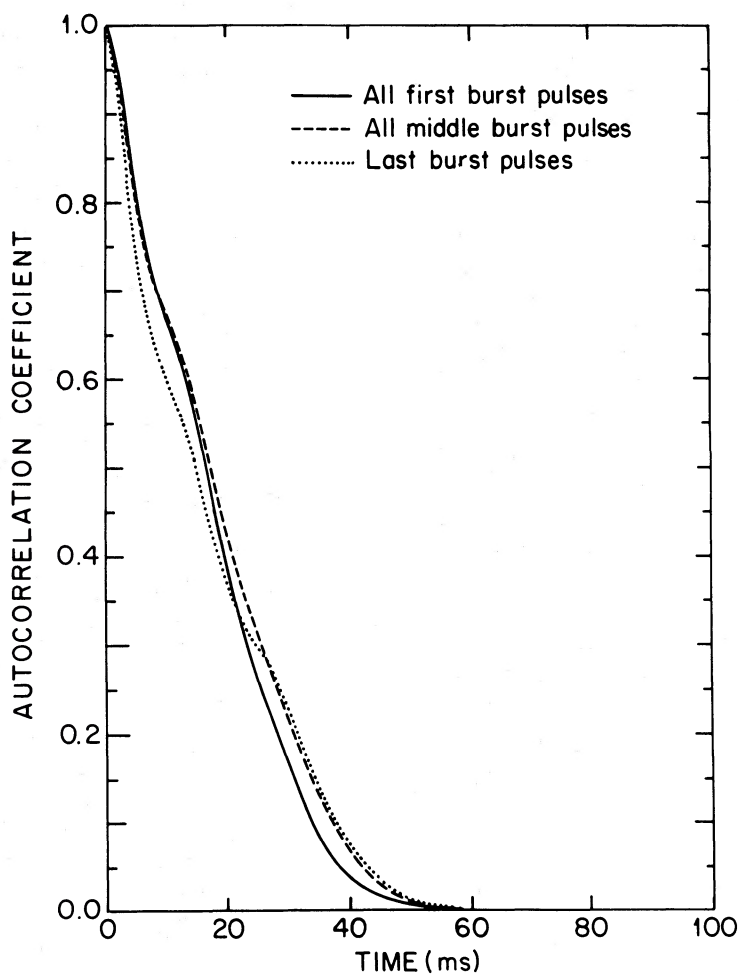


FIG. 8b

FIG. 8.—(a) Top panel: average pulse profiles of the first pulse in bursts (*dashed line*) all pulses between the first and last pulses (*solid line*); the last pulse in bursts (*dotted line*). Shaded region indicates maximum excursion of 10 subgroups of “middle” pulses from the average (*see text*). Bottom panel: all pulses identified as nulls. (b) Average autocorrelation functions for burst pulses divided up as in (a), first, middle, and end phases. Autocorrelation of the last pulse is $\sim 25\%$ narrower.

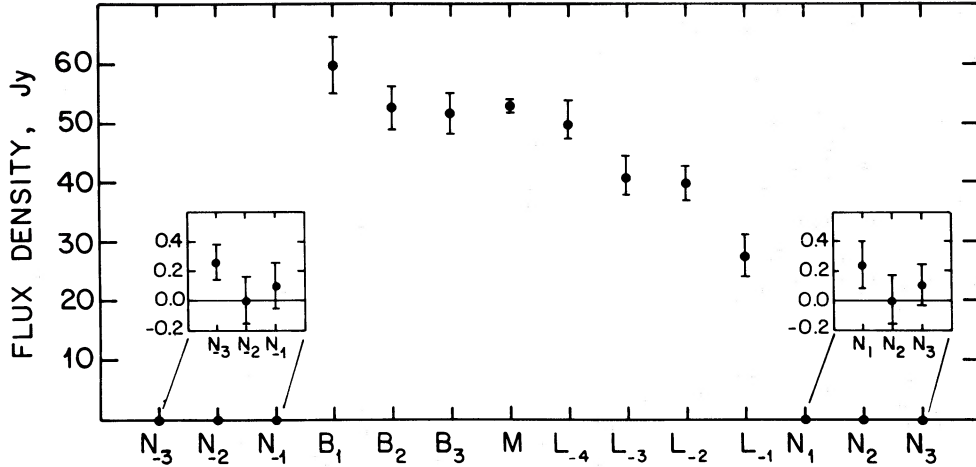


FIG. 9.—Flux density in bursts which were at least eight pulses long and preceded and followed by at least three null pulses. Preceding null pulses are labeled N_{-3}, N_{-2}, N_{-1} ; the first three burst pulses are labeled B_1, B_2, B_3 ; the middle pulses of a burst are lumped together and labeled M ; the last four burst pulses are labeled $L_{-4}, L_{-3}, L_{-2}, L_{-1}$; and the first three null pulses succeeding the burst are labeled N_1, N_2, N_3 . Last pulses of the burst are of significantly lower intensity than the middle pulses. (Note: for nulls of length 3, 4, and 5, some of the null pulses are counted twice: once as trailing a burst and then as preceding the next).

sity of the last burst pulse is

$$\langle I_B(L) \rangle = \frac{1}{P} \int_{t-P}^{tP} I_0 N(t) dt. \quad (4)$$

For PSR 1944 + 17, we modeled the null signature as a unit amplitude from pulse to pulse until t_0 , followed by an exponential decay:

$$N(t) = 1 - U(t - t_0)[1 - e^{-(t-t_0)/\tau}]. \quad (5)$$

Here U is the unit step function. This model predicts a ratio $\langle I_B(L) \rangle / \langle I_N(1) \rangle$ that is a function of τ and which we show in Figure 10. Using the mean ratio of 115 obtained from the data (and assuming a ratio $I_T/I_0 \approx 0.05-0.15$ for data we have used), we find a 3σ upper limit on the decay time, $\tau \leq 30$ ms.

The transition to the null state thus seems characterized by two time scales: a several-pulse-period decrease in flux density, followed by a rapid ($2 \text{ ms} < \tau < \text{subpulse decay time}$) transition to zero measurable emission.

We now consider the influence of the null signature on the observed pulse shape to see if we can assume that $N(t)$ is independent of the mechanism that determines the radiation beam. We therefore model the intensity during any single pulse as

$$I(t) = I_0 N(t - t_c) W(t), \quad (6)$$

where $I(t)$ is now the intensity at any point during the pulse period; $W(t)$ is the normalized average pulse wave form, assumed time independent in the corotating frame; and t_c is the fiducial point for the origin of the null and is a random variable uniformly distributed on $(0, P)$. Let us define the critical time t_{crit} as the t_c , such that the intensity integrated over the pulse equals the threshold intensity:

$$I_T = \int_t^{t+P} I_0 N(t' - t_{\text{crit}}) W(t') dt'. \quad (7)$$

Then the average wave form for the last burst pulse is

$$W_L(t) = \int_{t_{\text{crit}}-P}^{t_{\text{crit}}} N(t - t_c) W(t) dt_c. \quad (8)$$

As a simple example, we find for a boxcar wave form of width T

$$I_T = \frac{I_0}{P} \left\{ \left(t_{\text{crit}} + \frac{T}{2} \right) + \tau [1 - e^{-(T/2 - t_{\text{crit}})/\tau}] \right\}. \quad (9)$$

In the limit that $\tau \rightarrow 0$, we find that $t_{\text{crit}} = \epsilon P - T/2$, where $\epsilon \equiv I_T/I_0$, and that the pulse shape for the last pulse is simply

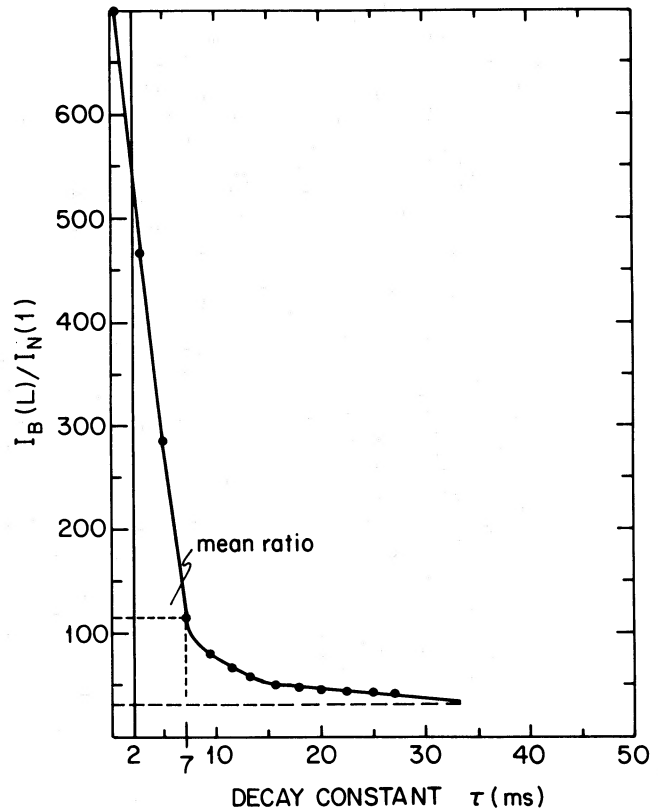


FIG. 10.—Ratio of the flux density of the last pulses in a model burst to the flux density of the first succeeding null pulse as a function of decay constant.

$W_B(t) = A(t)W(t)$, where

$$A(t) = \begin{cases} 1 & t \leq t_{\text{crit}} \\ 1 - \epsilon \left(\frac{t - t_{\text{crit}}}{T - \epsilon P} \right) & t > t_{\text{crit}} \end{cases} \quad (10)$$

The attenuation of the trailing edge is only a factor of $\epsilon \approx 0.05$ for the last $\Delta t = T/2 - \epsilon P$ of the pulse.

We numerically performed these calculations, using the actual wave form for $W(t)$, and found that exponential decay does not predict the observed shape of the last pulse. Using a value of 10 ms for τ , we find that the first component is not measurably attenuated, while the second component is attenuated by $\sim 5\%$. Decreasing τ does not significantly increase the attenuation, as one would expect from the boxcar example. A 5% attenuation leaves the final pulse profile within the spread of the average pulse profiles. Increasing τ to 30 ms attenuates the second component only slightly more than for $\tau = 10$ ms.

A different interpretation involves supposing that a null is the termination of subpulse production rather than a truncation of subpulses; in an idealized model, we assume that pulses contain 2 subpulses, except for the last burst pulse, which contains either 1 or 2 subpulses. The fraction with only 1 subpulse is equal to the probability that a null "occurs" during a time of order the subpulse duration $\sim \Delta t/P \approx 5\%$. The final burst pulse wave form is predicted to be

$$W_L(t) \approx (1 - \Delta t/P)W_2(t) + (\Delta t/P)W_1(t), \quad (11)$$

where $W_2(t)$ is the average wave form with 2 subpulses and $W_1(t)$ is the average wave form with 1 subpulse. Roughly 95% of the last burst pulses have 2 subpulses, and therefore the predicted wave form of the last burst pulse will still be approximately that of the average burst pulse, but the second half of the wave form is $\sim 5\%$ lower than that for typical burst pulses. It is actually up to 25% lower for some large subsets of the data (~ 3000 pulses, of which ~ 100 pulses are last pulses of bursts).

Our conclusion is that the shape of the final pulse in bursts is substantially different than the average wave form, and cannot be explained by a simple exponential decay modulation of the emission. Evidently, the mechanism which causes the null also changes the distribution of intensity in the pulse beam.

d) Transition to the Burst State

Using the intensity ratio of the last null pulse to the first burst pulse, we find (analogous to the argument above) that the rise time must be no more than 30 ms and the lack of sharp edges again implies it is at least 2 ms. The first pulse in a burst is substantially different from the last; in particular, it is not a mirror image of the last. Its intensity is at least as great as the average pulse, and the trailing wave form component is only $\sim 10\%$ attenuated, compared to the average wave form. Figure 8 suggests that the wave form is slightly narrower, has a smaller rise time, and begins faster than the average wave form. This could be due to a fast ($\tau < 10$ ms subpulse rise time) transition occurring in the pulse window. Alternatively, the emission may initially come from narrower regions and then spread (in the corotating frame). In contrast to the end of a burst, there is no second, longer time scale associated with the null-to-burst transition. Our main conclusion is that the transition to the burst state is quite different in character from the transition to the null state.

V. SUMMARY AND INTERPRETATION

We have identified three drift patterns in the pulsed intensity for PSR 1944+17 that are characterized by drift rates in the proportion of 1:2 for the organized A and B modes, and zero drift in the C mode. In addition, there is a fourth mode in which there is a chaotic phase relationship between pulses (i.e., no evident drifting). Changes from one mode to another are correlated with the occurrence of nulls. PSR 1944+17 shows no phase memory across nulls, in contrast to that found for PSR 0809+74, an object that shows only one highly organized mode of drifting (Unwin *et al.* 1978).

Transitions to the null state occur very rapidly on a time scale $2 < \tau < 30$ ms and correspond to a drop in intensity of at least a factor of 100. The null transition is preceded by a slow (~ 3 period) decay in average intensity of $\sim 50\%$. The last pulse before a null has a shape that is quantitatively different and more variable than the shapes of other pulses. Transitions from the null to burst state show the fast transition time, but show neither the slow change in intensity nor a difference in pulse shape that is seen at the end of a burst. It appears that the null transition is not an intensity modulation independent of subpulse and other fluctuations, but rather seems physically connected to the mechanism that determines the subpulse shape.

A good deal of stress has been placed on the strong phase memory observed between bursts from PSR 0809+74. The model of Ruderman and Sutherland (1975), as modified by Cheng and Ruderman (1977*a, b*, 1980), attributes memory to the creation of local hot spots on the magnetic polar cap of a neutron star. Heating is done by the Sturrock (1971) mechanism of pair creation from γ -rays in the magnetic field, causing a flow of highly relativistic electrons onto the polar cap. Thermionic emission from the surface depends sensitively on temperature, so ions are liberated far more easily from the hot regions. The ions are accelerated by the potential drop above the cap, and thermal X-rays from the hot cap pair-produce in the ions' Coulomb field. The ion current may fluctuate if the balance between pair production and thermionic emission is unstable. "Memory" may occur if the pair production restarts over hot spots. The model has been criticized (Filippenko and Radhakrishnan 1982) on the grounds that over the duration of a long null, many cooling times occur so that there is no preferential spot on the cap at which the next spark may begin, but one must regard estimates of cooling times of neutron star crusts with caution.

Filippenko, Readhead, and Ewing (1983) have also argued against the hot spot model because of the slight amount of phase drift observed across nulls from PSR 0809+74, in contrast to a presumed perfect memory (no phase shift) associated with hot spots. Perfect memory is expected, however, only if the radiation beam is rigidly locked to the source of radiating particles, which is true so long as the emission altitude does not vary. Such constancy of emission altitude seems unlikely since the particle density may be modulated during the null transitions, so some of the phase shifts may, in fact, result from altitude fluctuations of a few light milliseconds.

Arons (1983) has proposed a model that attributes drifting and nulling to the nutation of a radiation beam about some mean direction due to variations in induced current density, and the beam intensity is assumed to be nearly constant in time. The time scale for nutation is of order a rotation period

and is related to global changes in the pulsar magnetosphere rather than fluctuations local to the magnetic polar cap.

The nutation and hot-spot models are respectively representative of "angular beaming" and "temporal modulation" models that have been discussed for micropulse and subpulse emission (e.g., Rickett and Cordes 1981). The two time scales for pulse nulling from PSR 1944+17 do not unequivocally favor one model over another, but, in our judgment, seem to favor a temporal modulation picture. In a pure nutation model, the slow decrease in flux density might be associated with the slow nutation of the beam, while the fast dropout in intensity would imply a sharp edge to the beam. Such sharp edges would presumably be in the direction of magnetic latitude (i.e., in the plane containing $\hat{\Omega}$ = rotation axis and $\hat{\mu}$ = magnetic moment) which are not seen in the direction of magnetic longitude: average pulse shapes generally fall off slowly in pulse longitude, and, in some cases, emission is seen at low level through most of pulse longitude (e.g., Hankins and Cordes 1981; Rankin and Benson 1981).

In polar cap hot spot models, it is tempting to speculate that the slow decrease is related to a thermal time scale, while the quick transition corresponds to the system crossing a threshold for production of coherent radiation. For example, the slow variation may arise from an increase in temperature of the polar cap, accompanied by an increase in thermionic emission. Since, in the models of Cheng and Ruderman, thermionic emission decreases the vertical potential drop in the polar gap, pair production avalanches will cease once the temperature reaches a critical value. An alternate explanation is that the threshold may be in the plasma instability that is responsible for amplification of coherent radiation. In that case, perhaps only small variations in the energy densities of pairs and ions are needed to quench radiation. If one assumes that the physical regime for PSR 1944+17 is not fundamentally different from that for PSR 0809+74, however, then the phase memory across nulls in the latter object does suggest that the electric field in the gap changes dramatically in going from a burst state to a null state, as would be consistent if pair production is terminated during a null.

In the model of Filippenko and Radhakrishnan, nulling occurs by a transition from a condition of rapid spark discharges ($\sim 10^5 \text{ s}^{-1}$) to a condition of steady discharge, which

presumably leads to a termination of coherent emission. They postulate a slow decrease in the potential drop during sparking until steady discharge is reached; the slow decay observed in PSR 1944+17 might correspond to this slow decrease.

A model for the burst-null transition and subsequent turn-on of pulsars has been developed by Jones (1983). In the burst state, the electron flux onto the surface is initially dominated by electrons from pair creation. As the surface is heated and the mean surface nuclear charge falls, the flux due to photoelectrons (created by the ion current from the surface interacting with the blackbody radiation field) also grows. An instability arises when the photoelectron flux and surface temperature get sufficiently large. Thermionic emission and photoelectrons dominate the current flow, and the potential falls below that required for pair production. In the null state the mean nuclear charge grows, the ion emission decreases, and a transition to the burst state occurs. A time scale of $\sim 10^{-5} \text{ s}$ is predicted for the null-to-burst transition, and a time scale less than or equal to 0.2 s is predicted for the burst-to-null transition.

These distinct time scales are not able by themselves to explain the contrast in wave forms that we have found between the first and the last pulses of bursts for PSR 1944+17. However, the fact that the fast null transition may correspond to a cessation or strong alteration of subpulse formation underscores the suspicions of several workers (Lyne, Smith, and Graham 1971; Cheng and Ruderman 1980; Rickett and Cordes 1981) that subpulses are basic units in the pair avalanche process.

As a final note of caution, we point out that the time scales observed in the radio emission may differ substantially from those for particle injection because of mediating geometrical and transfer effects. These will probably increase the fluctuation times, so our values for null rise and decay are upper limits on those applicable to events near the polar cap.

This work was supported by the National Astronomy and Ionosphere Center, which is operated by Cornell University under contract with the National Science Foundation. T. H. Hankins acknowledges partial support from NSF grant AST 8217236. J. M. C. received support from the Alfred P. Sloan Foundation.

REFERENCES

- Arons, J. 1983, in *Positron-Electron Pairs in Astrophysics*, ed. M. L. Burns, A. K. Harding, and R. Ramaty (New York: American Institute of Physics), p. 163.
- Backer, D. C. 1970, *Nature*, **227**, 692.
- Cheng, A. F., and Ruderman, M. A. 1977a, *Ap. J.*, **212**, 800.
- . 1977b, *Ap. J.*, **214**, 598.
- . 1980, *Ap. J.*, **235**, 576.
- Drake, F. D., and Craft, H. D. 1968, *Nature*, **220**, 231.
- Filippenko, A. V., and Radhakrishnan, V. 1982, *Ap. J.*, **263**, 828.
- Filippenko, A. V., Readhead, A. C. S., and Ewing, M. S. 1983, in *Position-Electron Pairs in Astrophysics*, ed. M. L. Burns, A. K. Harding, and R. Ramaty (New York: American Institute of Physics), p. 113.
- Hankins, T. H., and Cordes, J. M. 1981, *Ap. J.*, **249**, 241.
- Huguenin, G. R., Taylor, J. H., and Troland, T. H. 1970, *Ap. J.*, **162**, 727.
- Jones, P. B. 1983, *M.N.R.A.S.*, **153**, 337.
- Lyne, A. G., and Ashworth, M. 1983, *M.N.R.A.S.*, **204**, 519.
- Lyne, A. G., Smith, F. G., and Graham, D. A. 1971, *M.N.R.A.S.*, **153**, 337.
- Manchester, R. N., and Taylor, J. H. 1977, *Pulsars* (San Francisco: Freeman).
- Popov, M. V., and Smirnova, T. V. 1982, *Soviet Astr.*, **26**, 439.
- Rankin, J. M., and Benson, J. M. 1981, *A.J.*, **86**, 418.
- Rickett, B. J., and Cordes, J. M. 1981, in *IAU Symposium 95, Pulsars*, ed. W. Sieber and R. Wielebinski (Dordrecht: Reidel), p. 107.
- Ritchings, R. T. 1976, *M.N.R.A.S.*, **176**, 249.
- Ruderman, M. A., and Sutherland, P. G. 1975, *Ap. J.*, **196**, 51.
- Sturrock, P. 1971, *Ap. J.*, **164**, 529.
- Taylor, J. H., and Huguenin, G. R. 1971, *Ap. J.*, **167**, 273.
- Unwin, S. C., Readhead, A. C. S., Wilkinson, P. N., and Ewing, M. S. 1978, *M.N.R.A.S.*, **182**, 711.
- Wright, G. A. E., and Fowler, L. A. 1981, *Astr. Ap.*, **101**, 356.

J. M. CORDES and W. T. S. DEICH: Astronomy Department and National Astronomy and Ionosphere Center, Space Sciences Building, Cornell University, Ithaca, NY 14853

T. H. HANKINS: School of Engineering, Dartmouth College, Hanover, NH 03755

J. M. RANKIN: Physics Department, University of Vermont, A405 Cook Building, Burlington, VT 05405